

Measurement of Flow Accelerated Corrosion Rate at an Elbow Pipe and Combination Effect of an Upstream Orifice

Yoichi UTANOHARA^{1,*}, Koichi KAMAHORI^{1,†}, Akira NAKAMURA¹ and Michio MURASE¹

¹ Institute of Nuclear Safety System, Inc., 64 Sata, Mihama-Cho, Mikata-Gun, Fukui 919-1205, Japan

ABSTRACT

Flow accelerated corrosion (FAC) rates at an elbow pipe with the diameter of $D = 50$ mm were measured by using corrosion sensors made of carbon steel. In addition, FAC rates at the elbow with an upstream orifice were measured to investigate the enhancement of FAC due to pipe geometries. The diameter ratio of the orifice was 0.5. The water temperature was 150 °C, the mean cross-sectional velocity was 4.98 m/s, the dissolved oxygen concentration was under 0.2 µg/kg, and pH was nearly neutral (about 7.0) at room temperature. The FAC rate was smaller at the intrados of the elbow pipe than at other circumferential locations due to low flow velocity near the inner surface. The ratio of the maximum FAC rate at the elbow pipe to the FAC rate in the straight pipe was about 3.7 without the upstream orifice and about 15.4 with the upstream orifice. This showed that the orifice significantly affected the FAC rate at the elbow pipe because of the short distance of $2.65D$ between the orifice and the elbow pipe.

KEYWORDS

flow accelerated corrosion, elbow pipe, wall thinning rate, electric resistance method, orifice

ARTICLE INFORMATION

Article history:

Received 18 January 2016

Accepted 30 March 2016

1. Introduction

Flow accelerated corrosion (FAC) is an important issue for aging management of fossil and nuclear power plants. FAC occurs at the pipe geometry where flow is strongly disturbed such as downstream from an orifice and at an elbow. FAC causes thinning of the pipe wall which occasionally leads to a pipe rupture accident. Thinning of pipe wall thickness had been managed based on non-destructive inspection of pipe wall thickness and evaluation of remaining lifetime following each electric utility's own guideline. The Japan Society of Mechanical Engineers published its guideline on pipe wall thinning management in 2005 [1]. Since then, the management method for pipe wall thinning has been unified under this guideline in Japan.

For prediction of FAC rates, it is important to understand factors influencing FAC. Generally, influencing factors are the water temperature, pH, dissolved oxygen concentration, material composition and fluid dynamics factor [2]. FAC studies from the viewpoint of the fluid dynamics factor (which the authors focus on) have mainly been evaluated by using the mean cross-sectional velocity [3][4], but recently the relationship between FAC and a local flow field has been reported [5]-[9]. The essential fluid dynamics factor influencing FAC is recognized to be the mass transfer coefficient near a pipe wall, and recent studies have been conducted based on this concept. To validate prediction methods for FAC rates, FAC data are needed. There are many power plant data but uncertainties for operation conditions and water chemistries are generally large. Therefore, the authors have measured FAC rates under well-controlled conditions in a test loop for the region downstream from an orifice and numerical simulations for the flow field in the experiments have been carried out [10]-[12]. The goal of these studies has been to develop a numerical simulation method by which effects of the local flow field on FAC can be evaluated.

In this study, the authors focused on FAC rates at an elbow pipe, because there are many elbows

*Corresponding author, E-mail: utanohara@inss.co.jp

†The Kansai Electric Power Co., Inc., 13-8 Goichi, Mihama-cho, Mikata-gun, Fukui 919-1141, Japan

in a power plant but FAC rates at an elbow pipe have not been directly measured in experiments, although the distribution of the mass transfer coefficient was measured experimentally [6] and wall thinning data in a power plant were examined [7]. The authors measured FAC rates at an elbow pipe with the diameter of 50 mm. Furthermore, the enhancement of FAC rate due to combinations of pipe geometries was investigated. Generally, if a certain pipe geometry exists upstream, the FAC rate at the downstream pipe geometry increases [13]. Hence, the FAC rates were compared at the elbow pipe with and without an orifice (the diameter ratio of 0.5) upstream from the elbow pipe. Experimental conditions were the water temperature of 150 °C and the mean cross-sectional velocity of 5.0 m/s.

2. Experimental Method

2.1. Test loop

The test loop is shown in Fig. 1. The experimental method was almost the same as in previous studies [10]-[12]; however, the test section was modified as described in Sec. 2.2. The recirculation pump was equipped downstream from the test section to avoid pump-induced disturbance effects on the test section. Dissolved oxygen concentration of the feed water was decreased by using the degasification unit before heating. Dissolved oxygen concentration was normally under 0.2 µg/kg during experiment. The pH was not controlled and was nearly neutral at room temperature with no additives. Iron concentration was kept constant at about 0.03 µg/g during the experiment by using the demineralizer. The loop temperature was automatically controlled by the heater power and cooling unit equipped in a small branch pipe downstream from the test section. Under the steady-state operation, cooling was needed to keep the water temperature constant due to Joule heating of the recirculation pump.

During the experiment, the pressure in the hot water tank, the water temperature and flow rate in the loop were measured. Dissolved oxygen concentration, conductivity and pH were measured at atmospheric pressure and room temperature by using the sampling system. The measurement instruments for water chemistries are listed in Table 1 [12].

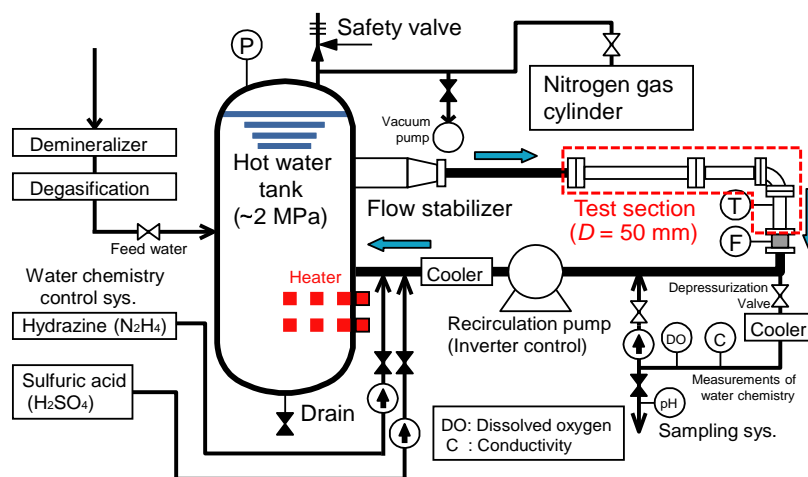


Fig. 1. Test loop for measurements of FAC rate

Table 1 Specifications of measurement instruments

Item measured	Manufacturer	Instrument model	Method
Dissolved oxygen	Nikkiso	7115-22	Membrane polarography
Conductivity	Nikkiso	9792	
pH	Horiba	D-51	Glass electrode
Iron concentration	Hach	Pocket colorimeter II	TPTZ

2.2. Test section

The test section for FAC rate measurement is shown in Fig. 2. The test section was made of stainless steel (SUS304) pipe which had an inner diameter of $D = 50\text{mm}$. The corrosion sensors were made of carbon steel plate (STPT42: Ni, 0.02 wt. %; Cr, 0.04 wt. %; Mo, 0.01 wt. %) and implanted on the pipe inner surface. Twenty corrosion sensors were installed: four at $9.25D$ upstream from the entrance of the elbow in the straight pipe, four at the center of the elbow pipe, four each at $2.68D$ and $3.68D$ downstream, and two each at $4.68D$ and $5.68D$ downstream from the exit of the elbow. It should be noted that the elbow pipe was bending in the horizontal plane, namely, the upstream pipe, the elbow pipe and the downstream pipe were placed in the horizontal plane.

The detailed geometry of the elbow pipe used in the experiment is shown in Fig. 3. Its geometry was different from that of normally used elbow types, because of the difficulty to install the corrosion sensors on the wall surface. In the previous studies [10]-[12], the inner surface of the test section was smoothed using a boring machine to remove undesirable bumps between the corrosion sensors and the pipe wall and to get a tight fit. However, such machining cannot be applied on the elbow surface. Hence, a straight part of 54 mm was sandwiched between two 45-degree elbows with the curvature radius of $R_e = 76.2\text{ mm}$ to install corrosion sensors. The equivalent curvature radius of the elbow pipe was $R_{ep} = 114.4\text{ mm}$.

In the case of the combination of the elbow pipe with the upstream orifice, the orifice plate was placed $2.65D$ upstream from the entrance of the elbow pipe. The profile of the orifice plate with the diameter ratio of $\beta = 0.5$ is shown in Fig. 4. The same orifice plate as that in the previous studies [10]-[12] was used to compare the FAC rates.

The layout of corrosion sensors as viewed from upstream is shown in Fig. 5. Four corrosion sensors were installed in the circumferential direction at the center of the elbow pipe. The directions were the upper, the lower, the extrados and the intrados of the elbow pipe. The corrosion sensors were insulated from the stainless steel pipe by a covering resin and were implanted on the pipe inner surface so that one surface of the plate was exposed to the fluid (hot water) as shown in Fig. 6.

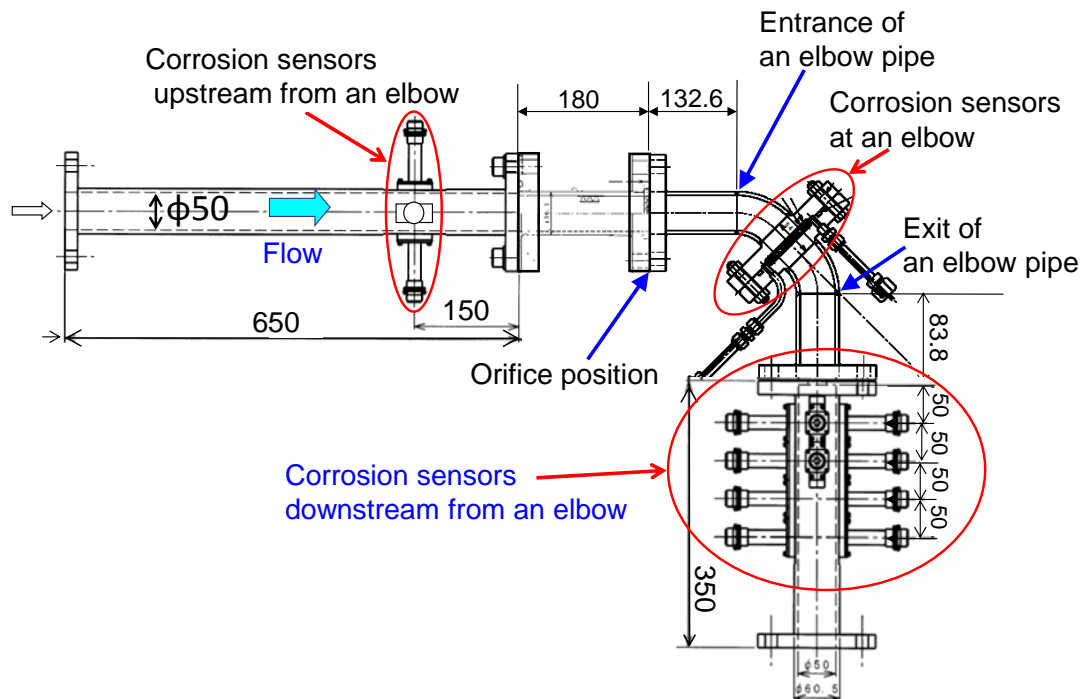


Fig. 2. Test section for measurements of FAC rate, overhead view (unit: mm)

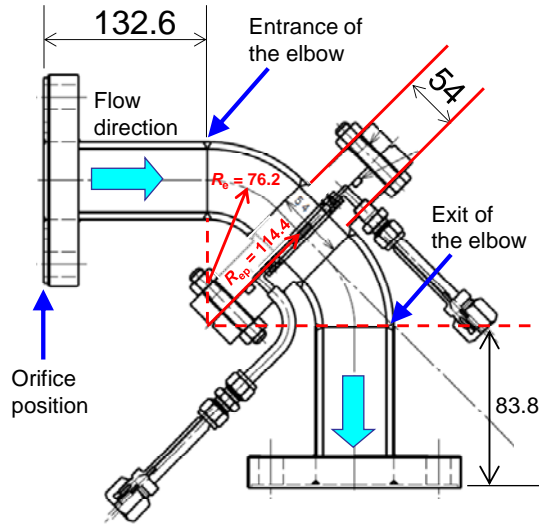


Fig. 3. Detailed geometry of the elbow pipe (unit: mm)

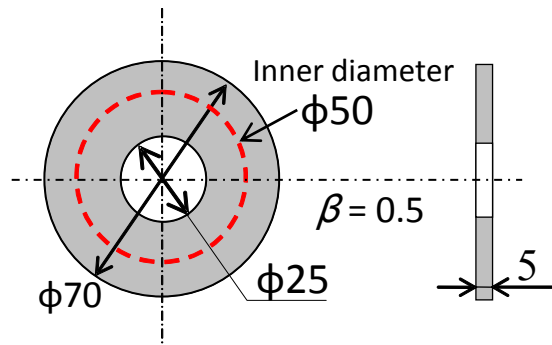


Fig. 4. Orifice plate (unit: mm)

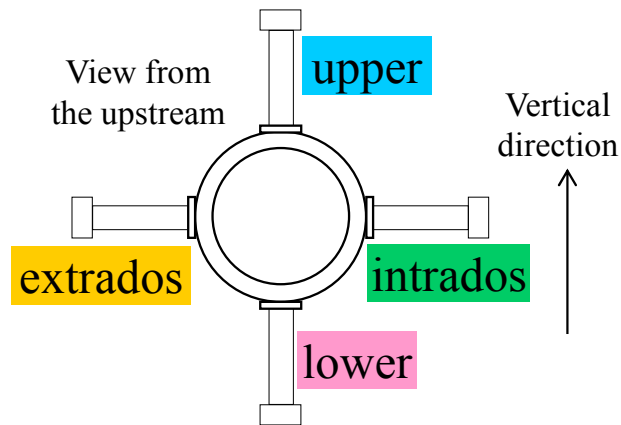


Fig. 5. Layout of sensors for measuring FAC rates

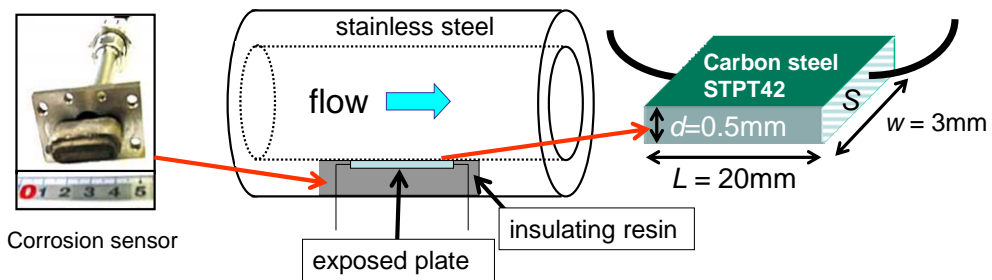


Fig. 6. Corrosion sensors

2.3. Measurement method for FAC rate

The FAC rate was measured by the electric resistance method. In the previous studies [10]-[12], a reference plate of the same material and same size as the exposed plate was used to compensate for the temperature change of resistance, but the reference plate was not used in this study. It is expected that failures of corrosion sensors would be reduced by simplifying the electrical-measuring circuit. The electric resistance of the sensor plate R is expressed by equation (1):

$$R = \rho_e \frac{L}{S} = \rho_e \frac{L}{d \cdot w} \quad (1)$$

where ρ_e , S , L , d and w are the electric resistivity, cross-sectional area, length, thickness and width of the sensor plate, respectively. While the simplified corrosion sensor has the advantage described above, the measured data are subject to more influence by temperature fluctuation because ρ_e depends on temperature. As described in Sec. 2.4, the temperature change during the experiment was within about ± 0.1 °C, then ρ_e can be treated as a constant value in this study. Hence, the thickness of the sensor plate d can be measured from the value of the electric resistance R and then the FAC rate of the sensor plate can be obtained from the gradient of the time history of metal loss, as shown in Sec. 3.1.

2.4. Measurement system for electric resistance

The measurement system for the electric resistance is shown in Fig. 7. This system consisted of corrosion sensors, a data acquisition system and a PC. The data acquisition system included 11 sets of data loggers (CorrLog, manufactured by CorrOcean), allowing measurement of the electric resistance of the corrosion sensors. There were 20 corrosion sensors in the test section (Fig. 2), but there only 11 data logger sets. In case of failures of corrosion sensors as mentioned in Sec. 2.3, the number of corrosion sensors was more than that of data loggers. Therefore, only 11 corrosion sensors were selected for measurement considering the necessity for understanding the FAC characteristics of the elbow. The monitoring software MultiTrend (CorrOcean), which manages the measurement data log, controls the measurement system and provides online monitoring, was used for data acquisition of the measured electric resistance values.

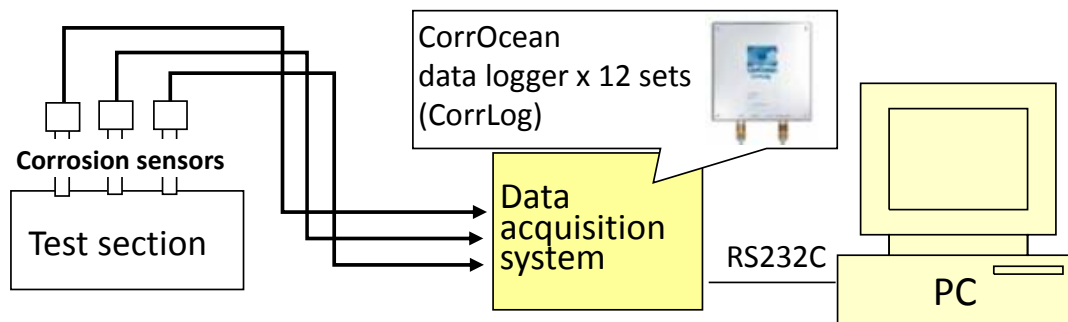


Fig. 7. Measurement system for the electric resistance

2.5. Experimental conditions

The FAC experimental conditions are shown in Table 2. The orifice upstream from the elbow pipe was not installed in Run 1, but it was installed in Run 2. The experimental period was 261 hours for Run 1 to obtain a thinning thickness of more than about 5 μm for reliable data and 100 hours for Run 2 because FAC rates were larger than those in Run 1. The mean cross-sectional velocity was about 5.0 m/s and its change during the experiment was within ± 0.3 %. The water temperature was about 149 °C and its change was within ± 0.1 °C. The water was pressurized to 1.5 MPa to avoid cavitation in the test loop. The dissolved oxygen concentration was almost always under 0.2 $\mu\text{g}/\text{kg}$. The pH was not controlled and was nearly neutral at room temperature. The difference of pH at each

sampling measurement was relatively large. Iron concentration increased a little initially and was kept constant at about 0.03 ± 0.01 $\mu\text{g/g}$ during the experiment.

Table 2. FAC experimental conditions

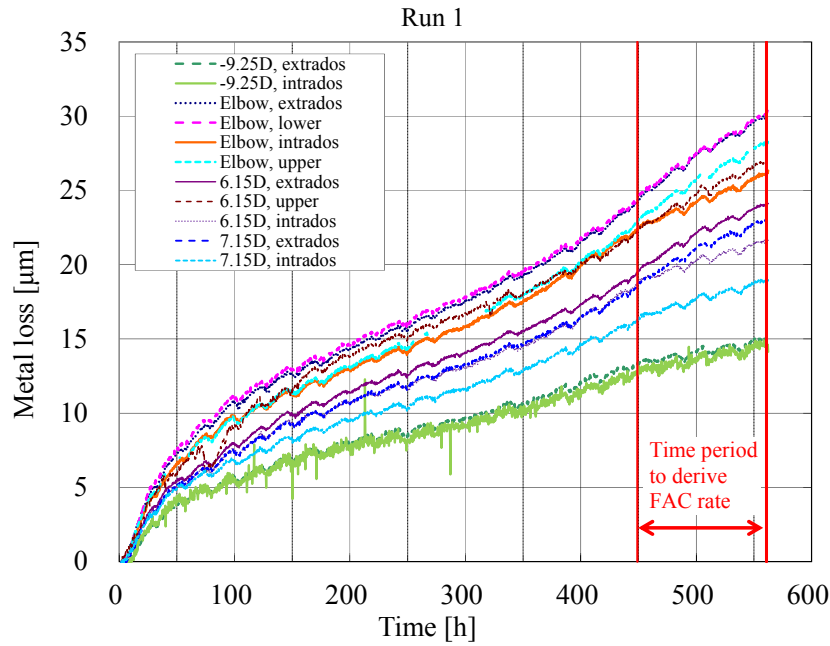
	Run 1	Run 2
Orifice diameter [mm]	-	25.0 ($\beta = 0.5$)
Experimental period [h]	261	100
Mean cross-sectional velocity [m/s]	4.98	4.98
Temperature [$^{\circ}\text{C}$]	149.2	149.3
Dissolved oxygen [$\mu\text{g/kg}$]	0.1	0.2
pH ^{*a}	7.0 (6.2 to 7.5)	7.0 (6.9 to 7.2)
Iron concentration [$\mu\text{g/g}$]	0.01 to 0.04	0.01 to 0.04
Corrosion sensor property	Carbon steel plates (STPT42: Ni, 0.02 wt. %; Cr, 0.04 wt. %; Mo, 0.01 wt. %)	

*a: The average during the corrosion measurement. The numbers in the parentheses are the minimum and the maximum of the measurement values.

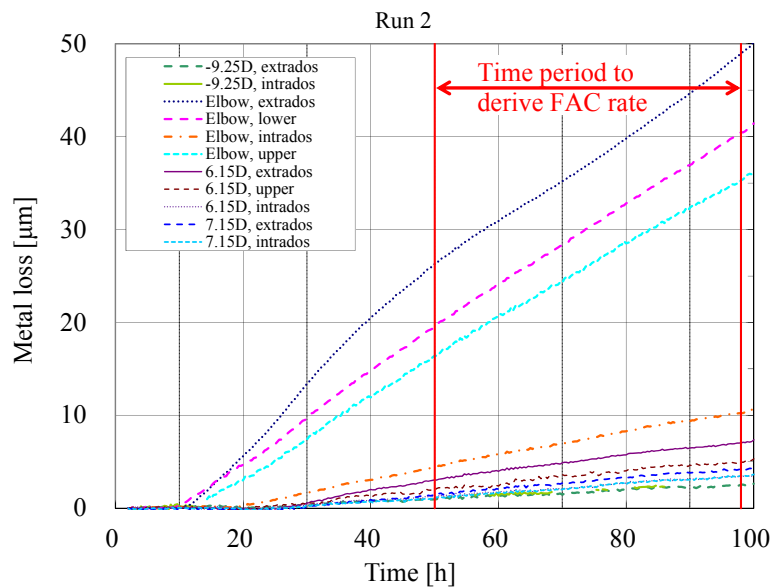
3. Experimental Results

3.1. Time history of metal loss

Time histories of metal loss of corrosion sensors in Run 1 and Run 2 are shown in Fig. 8. Descriptions in the legend are positions of the corrosion sensors. The origin of the longitudinal direction is the inlet of the elbow pipe. The metal losses changed with time and gradients became constant after a certain period of time. In Run 1, the gradients started to decrease after around 50 hours and then became relatively constant. In Run 2, the metal losses were small during the heating process, started to increase after 10-20 hours, and became almost linear after 20-40 hours. Compared with Run 2, the time histories in Run 1 had slight variations and they were a kind of noise mainly caused by change of atmospheric temperature. Since FAC rates in Run 1 were smaller than those of Run 2, variations became noticeable. The influence of noise can be reduced by time-averaging procedure. To obtain FAC rates after reaching steady state, the time-averaged increasing rate of the metal loss from 449 to 561 hours in Run 1 and from 50 to 98 hours in Run 2 was used. In Run 2, the metal loss at the elbow pipe was very large, and the experiment was finished before the metal loss at $-9.25D$ in the straight pipe reached about $5 \mu\text{m}$.



(a) Run 1



(b) Run 2

Fig. 8. Time histories of metal loss of corrosion sensors

3.2. FAC rates at the elbow pipe without the orifice

Figure 9 shows the distribution of FAC rates at the elbow pipe (Run 1, the case without the orifice). The mean cross-sectional velocity was 4.98 m/s. As mentioned in Sec. 3.1, time-averaged values are plotted in Fig.9. Their standard deviations (not shown in the figure) were 0.3 to 0.5 mm/y and comparable with time-averaged values, but influence of variation were reduced and tendency can be extracted by time-averaging procedure. The FAC rate was smaller at the intrados of the elbow pipe than at other circumferential locations. This seemed to be due to the velocity distribution in the elbow. Generally, secondary flow is induced in the elbow because of the centrifugal force through the elbow radius and faster flow moves to the extrados. Hence flow velocity near the intrados at the middle part of the elbow is relatively low. The possible reason for the low FAC rate of the intrados at the elbow was likely related to the low velocity near the inner surface. The FAC rates at the elbow pipe were

larger than those upstream and downstream from the elbow pipe and the FAC rates downstream from the elbow pipe decreased along the flow direction. The tendency of low FAC rate at the intrados side continued downstream from the elbow. These results indicated that the velocity distribution, low near the intrados and high near the extrados, was still retained downstream. The ratios of the maximum FAC rate at each x/D to the FAC rate in the straight pipe ($x/D = -9.25$) were respectively about 3.7, 2.8 and 2.7 for $x/D = 1.74, 6.15$ and 7.15 .

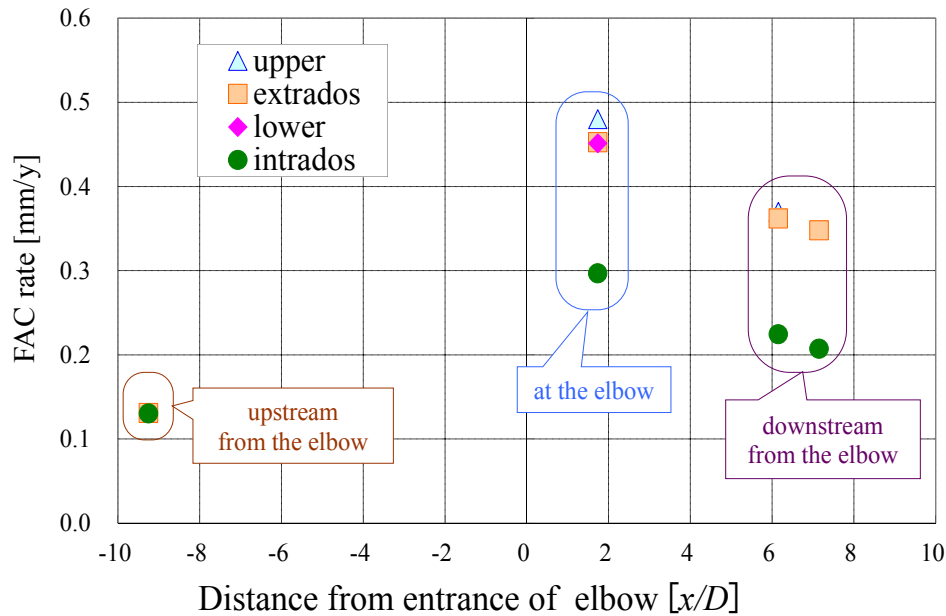


Fig. 9. FAC rates at the elbow pipe without orifice (Run 1)

3.3. FAC rates at the elbow pipe downstream from the orifice

The FAC rates of the elbow pipe downstream from the orifice with the diameter ratio of $\beta = 0.5$ (Run 2) were measured under the conditions of the same measuring positions and velocity of about 5.0 m/s as those in Run 1 (described in Sec.3.1), and the results are shown in Fig. 10. Standard deviations (not shown in the figure) were 0.15 to 0.38 mm/y and smaller than time-averaged values, particularly at the elbow in Fig. 10. Overall, FAC rates increased compared with Run 1, the case without the upstream orifice. The FAC rate was smaller at the intrados of the elbow pipe than at other circumferential locations like that in Run 1, but the circumferential difference of FAC rates was small at $x/D = 6.15$ and 7.15 unlike Run 1. The ratios of the maximum FAC rate at each x/D to the FAC rate in the straight pipe ($x/D = -9.25$) were respectively about 15.4, 2.8 and 1.9 for $x/D = 1.74, 6.15$ and 7.15 . The comparison with those in Run 1 (3.7, 2.8 and 2.7) showed that the orifice largely affected the FAC rate at the elbow pipe ($x/D = 1.74$) but did not affect the FAC rate so much at $x/D = 6.15$ and 7.15 .

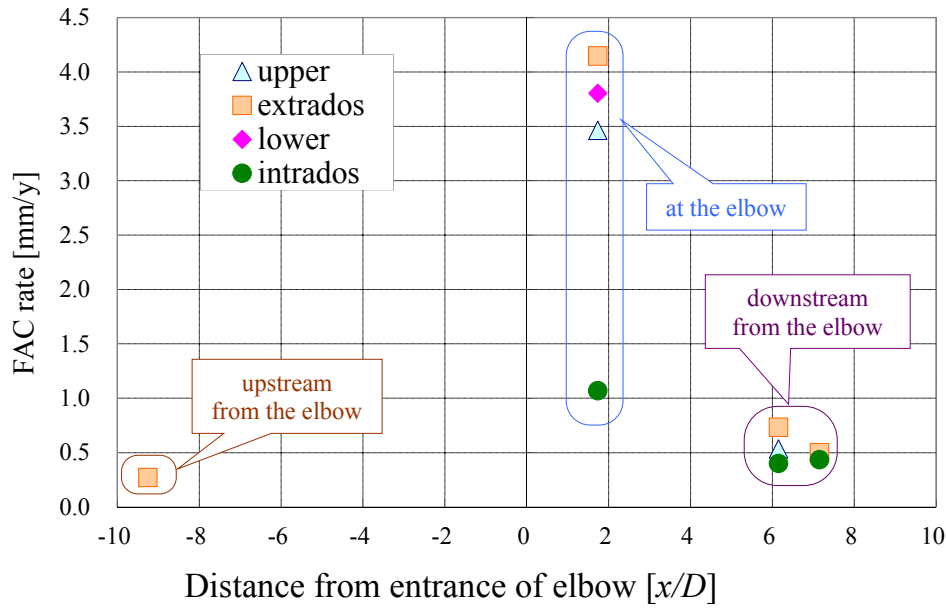


Fig. 10. FAC rates at the elbow pipe downstream from the orifice (Run 2)

4. Discussion

Figure 11 compares FAC rates in Run 2 with those downstream from the single orifice without the elbow [11]. The locations of corrosion sensors with the single orifice were 1, 2, 3 and 4D downstream from the orifice outlet. This comparison showed that the FAC rate at 2.65D downstream from the orifice ($x/D = 0$ in Fig. 11) was large and the effect of the upstream orifice was strong at the entrance of the elbow pipe. The maximum increase in the FAC rate due to the elbow pipe from the single orifice case was about 1.2 mm/y ($= 4.2 \text{ mm/y} - 3.0 \text{ mm/y}$) and was about 3.4 times that in Run 1 of the single elbow case ($0.48 \text{ mm/y} - 0.13 \text{ mm/y} = 0.35 \text{ mm/y}$, Fig. 9). This showed that the combination of an orifice and an elbow pipe with the short distance of 2.65D promoted the FAC rate at the elbow pipe.

To understand the influence of the upstream orifice, the measured and predicted orifice flow fields [10] are shown in Figs. 12 and 13. In the case of the single orifice, the reattachment point was around 2.5D downstream from the orifice. Flow structures such as the velocity distribution did not depend on the mean cross-sectional flow velocity U_{ave} when normalized by U_{ave} . From Fig. 13, the orifice jet continued around 3D downstream from the orifice. Hence, in the present study of the orifice and elbow combinations, the distance 2.65D downstream from the orifice was just behind the reattachment point and the orifice jet probably reached the elbow extrados. This jet flow might enhance the FAC rate at the elbow. It is expected that FAC rates at the elbow pipe with the distance over 4D between the orifice and the elbow pipe may be mitigated, because the FAC rate at 4D was about 40 % of that at 1D to 3D downstream from the orifice, and also the orifice jet in Fig. 13 disappeared at 4D downstream.

According to the above discussion, the orifice and elbow were combined at the most effective location. Kastner et al. [13] proposed a formula of combination effect and an upstream component A with geometry factor $k_{c,A}$ affects a downstream component B with geometry factor $k_{c,B}$. The increase of downstream geometry factor is described as follow:

$$\Delta k_{c,A} = k_{c,A} \exp(-C \cdot z / D). \quad (2)$$

Here, z is distance between component A and B, and C is constant ($= 0.231$). The total geometry factor of downstream component $k'_{c,B}$ is

$$k'_{c,B} = k_{c,B} + \Delta k_{c,A}. \quad (3)$$

The influence of upstream component becomes the maximum when $z/D = 0$ and $k'_{c,B}$ equals the sum of $k_{c,A}$ and $k_{c,B}$. In the present study, the sum of FAC rates of the single orifice (about 3.0 mm/y) and the elbow in Run 1 (about 0.5 mm/y) was comparable with the FAC rate of the downstream elbow in Run 2 (about 4.0 mm/y). In this way, the results of this study agreed with the formula proposed by Kastner et al. [13].

The discussion here is based on the previous results of the single orifice case [10]. To understand the combination effect of the upstream orifice and downstream elbow, numerical simulation of this combination is needed and it remains as future work.

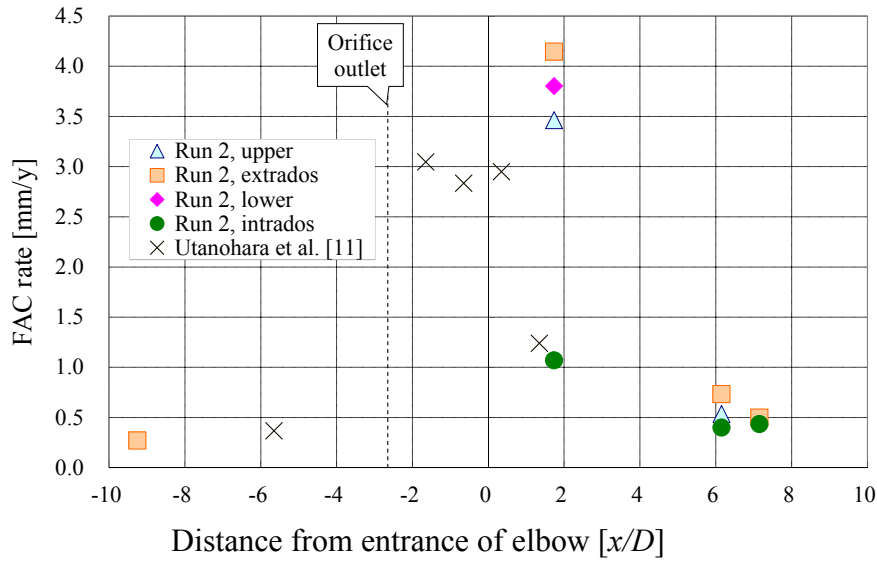


Fig. 11. Comparison of FAC rates in Run 2 with those downstream from single orifice

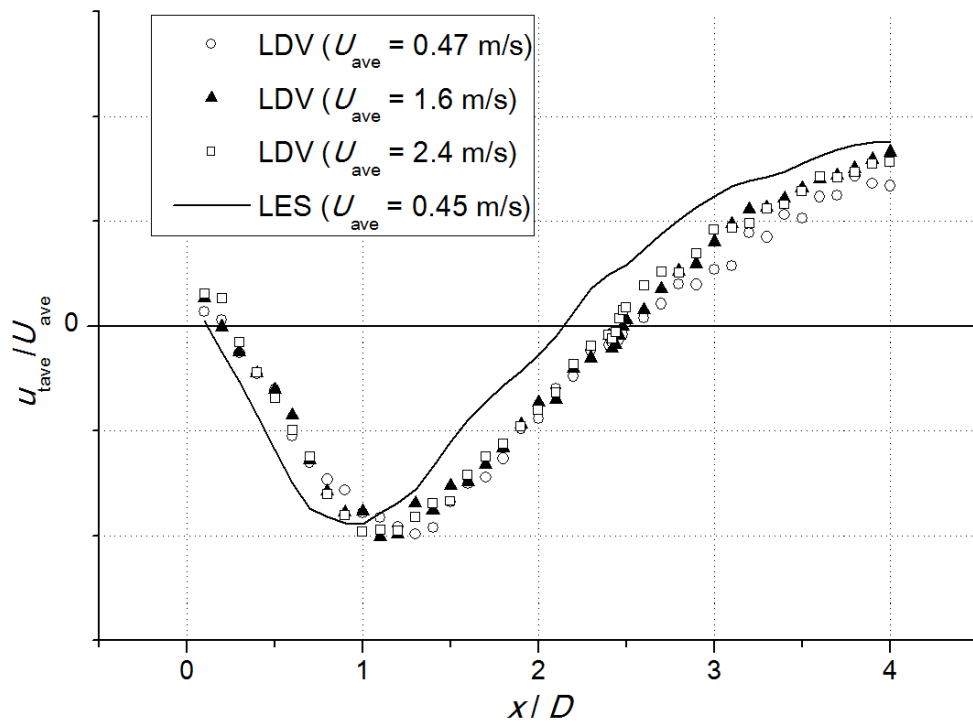


Fig. 12. Axial velocity profiles near the wall ($y = 1$ mm from the wall) downstream from the single orifice [10]

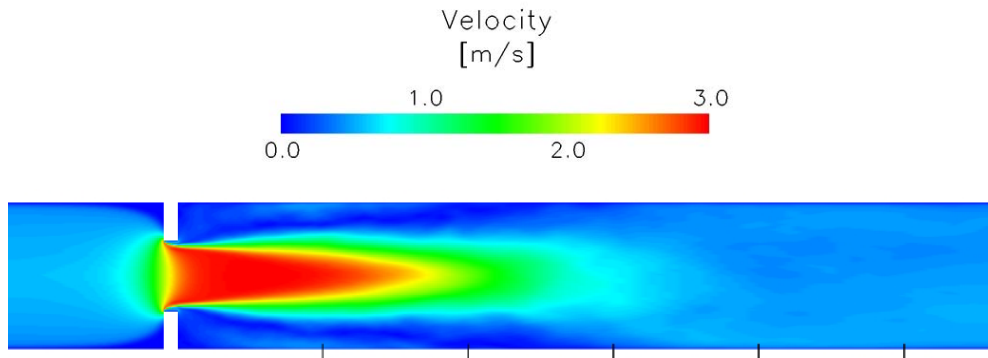


Fig. 13. Time-averaged velocity distribution of the orifice flow ($U_{ave} = 0.453$ m/s) predicted by large eddy simulation [10], tick marks are placed every $1D$ distance

5. Conclusions

In this study, the authors measured FAC rates at an elbow pipe. In addition, to understand the enhancement of FAC rate by the combination of pipe geometries, FAC rates with and without an orifice (respectively Run 2 and Run 1) upstream from the elbow pipe were compared with each other. The following conclusions were obtained.

- 1) In Run 1 and Run 2, FAC rates at the elbow pipe were larger than those upstream and downstream from the elbow pipe. The FAC rate was smaller at the intrados of the elbow pipe than at other circumferential locations. This might be due to the low velocity near the intrados. FAC rates downstream from the elbow pipe decreased along the flow direction.
- 2) In Run 1 (without the upstream orifice), the ratio of the maximum FAC rate at the elbow pipe to the FAC rate in the straight pipe was about 3.7.
- 3) In Run 2, when the orifice was $2.65D$ upstream from the elbow pipe, the ratio of the maximum FAC rate at the elbow pipe to the FAC rate in the straight pipe was 15.4. The comparison of the value of 15.4 with the value of 3.7 in Run 1 showed that the orifice largely affected the FAC rate at the elbow pipe.
- 4) The comparison of FAC rates in Run 2 with those downstream from the single orifice without the elbow showed that the effect of the upstream orifice was strong at the entrance of the elbow pipe because the FAC rate at $2.65D$ downstream from the orifice was still large. The maximum increase in the FAC rate due to the elbow pipe of about 1.2 mm/y in Run 2 was about 3.4 times that in Run 1 (0.35 mm/y) and this showed that the combination of an orifice and an elbow pipe with a short distance promoted the FAC rate at the elbow pipe.

References

- [1] Japan Society of Mechanical Engineers: “Rules on Pipe Wall Thinning Management”, JSME S CA1-2005 (2006).
- [2] R. B. Dooley, V. K. Chexal: “Flow-Accelerated Corrosion of Pressure Vessels in Fossil Plants”, *International Journal of Pressure Vessels and Piping*, Vol. 77, No. 2-3, pp.85-90, (2000).
- [3] G. J. Bignold, K. Garbett, R. Garnsey, I. S. Woolsey: “Erosion-Corrosion in Nuclear Steam Generators”, *Water Chemistry of Nuclear Reactor Systems 2*, British Nuclear Engineering Society, pp. 5-18, (1981).
- [4] H. G. Heitmann, P. Schub: “Initial Experience Gained with a High pH Value in the Secondary System of PWRs”, *Water Chemistry of Nuclear Reactor Systems 3*, Vol. 1, British Nuclear Engineering Society, pp. 243-252, (1983).
- [5] K. Yoneda, T. Ohira, K. Tanji, S. Akiba, K. Niiyama, R. Morita, F. Inada: “Evaluation of Hydraulic Factors Affecting Flow Accelerated Corrosion and Its Verification with Power Plant Data”, *Proceedings of the ASME 2009 Pressure Vessels and Piping Division Conference (PVP2009)*, Prague, Czech Republic, July 26–30, No. PVP2009-77486, (2009).
- [6] M. El-Gammal, H. Mazhar, J. S. Cotton, C. Shefski, J. Pietralik, C. Y. Ching: “The Hydrodynamic Effects

- of Single-phase Flow on Flow Accelerated Corrosion in a 90-degree elbow”, *Nuclear Engineering and Design*, Vol. 240, pp.1589-1598, (2010).
- [7] M. J. Pietralik, S. C. Schefski: “Flow and Mass Transfer in Bends under Flow-Accelerated Corrosion Wall Thinning Conditions”, *ASME Journal of Engineering for Gas Turbines and Power*, Vol. 133, pp.012902, (2011).
- [8] N. Fujisawa, T. Yamagata, S. Kanno, A. Ito, T. Takano: “The Mechanism of Asymmetric Pipe-Wall Thinning behind an Orifice by Combined Effect of Swirling Flow and Orifice Bias”, *Nuclear Engineering and Design*, Vol. 252, pp. 19-26, (2012).
- [9] T. Tsuneyoshi, K. Kamiya, T. Ito, Y. Tsuji: “Measurement of mass transfer coefficients and analyses of turbulent scalar transport with LES behind the orifice in a circular pipe”, *Transactions of the JSME*, Vol. 81, No. 828, (2015), DOI:10.1299/transjsme.15-00162. (in Japanese)
- [10] Y. Utanohara, Y. Nagaya, A. Nakamura, M. Murase: “Influence of Local Flow Field on Flow Accelerated Corrosion Downstream from an Orifice”, *JSME Journal of Power and Energy Systems*, Vol. 6, No. 1, pp. 18-33, (2012).
- [11] Y. Utanohara, Y. Nagaya, A. Nakamura, M. Murase, K. Kamahori: “Correlation between Flow Accelerated Corrosion and Wall Shear Stress Downstream from an Orifice”, *JSME Journal of Power and Energy Systems*, Vol. 7, No. 3, pp. 138-147, (2013).
- [12] K. Kamahori, Y. Utanohara, A. Nakamura, M. Murase, Y. Nagaya: “Flow Accelerated Corrosion Downstream from an Orifice (1.Measurement of Corrosion Rate)”, *Proceedings of the Conference on Flow Accelerated Corrosion (FAC2013)*, Avignon, France, May 21-24, No.1234, (2013).
- [13] W. Kastner, M. Erve, N. Henzel, B. Stellwag: "Calculation Code for Erosion Corrosion Induced Wall Thinning in Piping Systems", *Nuclear Engineering and Design*, Vol. 119, No. 2-3, pp. 431-438 (1990).